Electrochimica Acta 55 (2010) 8422–8429

Contents lists available at ScienceDirect

Electrochimica Acta

journal homepage: www.elsevier.com/locate/electacta

The influence of tetrapod-like ZnO morphology and electrolytes on energy conversion efficiency of dye-sensitized solar cells

Chia-Hua Lee[a,d], Wei-Hao Chiu[b], Kun-Mu Lee[a,e], Wen-Hsiang Yen[a], Hsiu-Fen Lin[c], Wen-Feng Hsieh[b], Jenn-Ming Wu[d,*]

[a] Green Energy and Environment Research Laboratories, Industrial Technology Research Institute, Hsinchu 310, Taiwan, ROC
[b] Department of Photonics & Institute of Electro-Optical Engineering, National Chiao Tung University,1001 Tahsueh Road, Hsinchu 300, Taiwan
[c] Material and Chemical Research Laboratories, Industrial Technology Research Institute, Hsinchu 310, Taiwan, ROC
[d] Department of Materials Science and Engineering, National Tsing-Hua University, 101, Sec. 2, Hsinchu 300, Taiwan
[e] Department of Applied Chemistry, Providence University, 200 Chungchi Rd. Shalu, Taichung Hsien 433, Taiwan

ARTICLE INFO

Article history:
Received 21 May 2010
Received in revised form 23 July 2010
Accepted 23 July 2010
Available online 1 August 2010

Keywords:
ZnO
Dye-sensitized solar cell
EIS
Dc thermal plasma
Electrolyte additive

ABSTRACT

Tetrapod-like ZnO nanostructures prepared by dc plasma technology were used as photoelectrodes in dye-sensitized solar cells (DSSCs). Each of the tetrapod-like ZnO possesses four extended arms that offer improved electron transport properties. Tetrapod-like ZnO with short (S-ZnO) and long arms (L-ZnO) were synthesized by controlling the plasma gas flow and the input power. Between these two tetrapod-like ZnO nanopowders, the DSSCs using S-ZnO showed higher energy conversion efficiency than using L-ZnO. This is due to the resulting increase in dye adsorption and enhanced short-circuit current density, using S-ZnO. Electrochemical impedance spectroscopy (EIS) shows that the properties of electron transport of S-ZnO are superior to that of the L-ZnO. We investigated the effect of the redox electrolytes (I_2) and the additives (LiI and TBP) on the performance of the DSSCs by intensity-modulated photovoltage spectroscopy and EIS.

1. Introduction

Dye-sensitized solar cells (DSSCs) are regarded as promising low cost solar cells with high light to energy conversion efficiency, due to their relative inexpensive manufacturing processes. A light to energy conversion efficiency of more than 11% has been achieved by TiO_2 nanoparticles film sensitized by a ruthenium-based dye systems [1,2]. However, electrons transport through the TiO_2 nanoparticle network by a slow trap-mediated diffusion, which limits the performance of the device [3]. In order to improve the performance of DSSCs, parameters such as morphology and the physical properties of nanocrystalline oxide films, photochemical properties of molecular sensitizers, and electrochemical characteristics of redox electrolytes need to be investigated more intensively [4,5].

Other metal oxides like SnO_2, In_2O_3, Nb_2O_5, and ZnO have also been used as photoelectrodes for DSSCs [6–8]. Among these oxide materials, the band gap and the energetic position of ZnO are similar to those of TiO_2 [9]. In addition to traditional photoelectrodes constructed of nanoparticles, many researchers have shown that the morphology of photoelectrodes plays an important role in optimizing the performance of DSSCs [10–19]. In recent years, several interesting photoelectrode architectures of ZnO have been investigated intensively, for improved electron transport properties or increased light harvesting in recent years. Photoelectrodes constructed from one-dimensionally (1D) structured semiconductor metal oxides such as ZnO nanowires and nanotubes enhance electron transport properties due to their stretching structure in specified directions and decreased number of intercrystalline contacts [11,12]. However, the relatively low surface area for dye adsorption leads to insufficient light harvesting and limited cell performance [13]. To increase the light harvesting of ZnO nanowire-based DSSCs, photoelectrodes comprising hybrid ZnO nanoparticles and nanowires have been introduced. The overall efficiency consequently improved to 2.4% [14]. In addition to the one-dimensionally structured ZnO, the overall efficiency of the DSSCs based on ZnO nanoflowers and ZnO nanosheets was also raised to 1.9% and 3.9%, respectively [15,16]. The overall efficiency of 3.5–5.4% was further achieved by using the hierarchically structured ZnO films, providing a large internal surface area for dye loading and light scattering, to enhance light absorption [17–19].

One-dimensional nanorods/nanowires are thought to have better electron transport properties and more efficient carrier collection capability. Various synthetic techniques such as wet-

* Corresponding author. Tel.: +886 3 5162227; fax: +886 3 5722366.
E-mail address: wu408410@yahoo.com.tw (J.-M. Wu).

0013-4686/$ – see front matter © 2010 Elsevier Ltd. All rights reserved.
doi:10.1016/j.electacta.2010.07.061

chemistry routes and vapor deposition processes have been developed to fabricate ZnO 1D nanostructures [20]. Fabricate solution-based ZnO nanowires with a length of 10 μm, requires a lot of time. The other drawback is their relatively low overall efficiency, due to low surface area. Recently, significant improvements in electron transport and overall performance of ZnO-based DSSCs have been achieved using tetrapod ZnO photoelectrodes, which decrease the number of the intercrystalline contacts between grain boundaries [21]. A high performance/price ratio of photovoltaic devices is widely regarded as essential for future applications. Therefore, high yield synthesis of extended 1D structured material with good electron transport is important in the application of the DSSCs.

Although ZnO has a similar band energy structure to TiO_2, the conversion efficiency of ZnO-based devices was reported to be lower than that of the TiO_2-based ones. The additives in the electrolyte affected the energetic of the photoelectrode and the performance of the DSSCs [22–26]. However, most studies were related to TiO_2 DSSCs with few reports on ZnO DSSCs. To improve the performance of the ZnO DSSCs, it would be worthwhile to investigate the effects of additives in the electrolyte on ZnO DSSCs.

In this paper, we present a rapid, continuous method for the fabrication of tetrapod-like ZnO nanostructures as photoelectrodes for DSSCs, by dc thermal plasma synthesis. The fabricated tetrapod-like ZnO nanostructures possess a high degree of crystallinity, as well as a distinctive structure, with extended arms wedged within a network of ZnO film to provide a direct path for electron transport. To improve the light harvesting efficiency of the ZnO DSSCs, the tetrapod-like ZnO should have suitable size and surface area. We present the effects of the thickness and morphology of the tetrapod-like ZnO photoelectrodes on the performance of the DSSCs in this investigation. In addition, we discuss the influences of electrolyte additives including Li^+ ions, I^-/I_2 redox couple, and *tert*-butylpyridine (TBP).

2. Experimental

2.1. Synthesis and characterization of tetrapod-like ZnO

Tetrapod-like ZnO nanostructures were synthesized using a dc plasma reactor [27]. The plasma was formed by N_2 gas in the reactor. Commercial metal zinc wires with a diameter of 1.2 mm and purity above 99.9% (Praxair) were used as the raw material. Zinc wires were fed into a plasma system through carrier gas (air) under a fixed flow rate of 10 slm. They subsequently underwent vaporization, oxidation, and quenching processes to form tetrapod-like ZnO nanostructured powders. The size of the particles comprising the nanopowders varied with the flow rate of the plasma gas (N_2) and the input power. After the plasma synthesis process, large quantities of white nanopowders were collected in the cold zone of the reactor.

2.2. Preparation of photoelectrodes and solar Cells

Two tetrapod-like ZnO powders of different sizes were dispersed in α-terpineol (Fluka) with equal proportions of ethyl cellulose as a binder to form two ZnO pastes. Two ZnO photoelectrode films were prepared from the two ZnO pastes by screen-printing on fluorine doped tin oxide (FTO) substrates (3 mm thickness, 8–10 Ω/□, Nippon Sheet Glass). The photoelectrodes were heated at 400 °C for 1 h. The area of the active electrode was typically 0.28 cm^2. Dye-loaded ZnO electrodes were prepared by immersing the ZnO photoelectrodes in a solution of 0.5 mM *cis*-bis(isothiocyanato)bis-(2,2′-bipyridyl-4,4′-dicarboxylato)-ruthenium(II) bis-tetrabutylammonium (Solaronix, N719) in a mixed solvent of 1:1 acetonitrile and *tert*-butanol for 20 min. The dye-loaded electrodes were then rinsed with acetonitrile. The dye-loaded electrodes were sandwiched together with thermally platinized FTO counter electrodes separated by 60-μm-thick hot-melt spacers (Dupont, Surlyn). The internal space of the cell was filled with an electrolyte solution containing an iodine redox couple consisting of 1,1-methyl-3-propylimidazolium iodide (PmII), I_2, LiI, and *tert*-butylpyridine (TBP) in acetonitrile (AN).

2.3. Instrumentation

The morphology and dimensions were observed by a field emission scanning electron microscope (FESEM) (JEOL, JSM-7000F) operating at 10 keV, and a field emission transmission electron microscope (FETEM) (JEOL, JEM-2100F) operating at 200 keV. The phases were characterized using a Bade D1 thin film X-ray diffractometer. The thickness of the photoelectrodes was measured by a Microfigure Measuring Surfcorder (Kosaka Laboratory, ET3000). The surface area was determined with the Brunauer–Emmett–Teller (BET) equation, using a Micromeritics ASAP 2000 at 77 K. The overall energy conversion efficiency was evaluated using a xenon lamp (Yamashita Denso, YSS-100A) with a light intensity 100 mW cm^{-2} (AM1.5). The current–voltage characteristics of the devices were scanned from 0 V to 0.9 V with 0.03 V/s sweep speed and 0.018 V step voltage. The incident light intensity was calibrated with a standard silicon photodiode (Bunko Keiki, BS-520). Evolution of the electron transport process in the cell with different additives and concentrations was investigated through intensity-modulated photovoltage spectroscopy (IMVS) and electrochemical impedance spectroscopy (EIS). The ac impedance spectroscopy was carried out by an electrochemical analyzer (Autolab, PGSTAT30).

3. Results and discussion

3.1. Characterization of tetrapod-like ZnO

Fig. 1 shows the morphology and the structure of the plasma synthesized tetrapod-like ZnO nanopowders. A typical SEM image shown in Fig. 1(a) illustrates that the ZnO nanocrystals were either tetrapod shaped or rod-like. Fig. 1(b) displays a FETEM image taken from the core center of a tetrapod ZnO, demonstrating that the tetrapod ZnO contains four arms: one perpendicular to and three parallel to the image.

The plasma gas flow rate affected the proportion of tetrapod-like to rod-like of ZnO nanoparticles as well as the length of the tetrapod arms of ZnO. Fig. 2 shows SEM images of ZnO obtained under different carrier gas flow rates. At a plasma gas flow rate of 70 slm and input power of 70 kW, the arm length of the tetrapod ZnO nanocrystals synthesized (L-ZnO) were in the range of 100–900 nm and with an average length of 380 nm, as shown in Fig. 2(a). The L-ZnO contained 45% tetrapod shaped ZnO. When the plasma gas flow rate increased to 90 slm and the input power increased to 90 kW, the arm length of the tetrapod ZnO nanocrystals (S-ZnO) decreased to approximately 30–250 nm with an average length of 140 nm, as shown in Fig. 2(b). The S-ZnO contained 65% tetrapod shaped ZnO. The diameter of the ZnO nanoparticles, which did not change significantly with changes in the carrier gas flow rate, was an average of approximately 50 nm. Fig. 2(c) shows the XRD patterns of the L-ZnO and S-ZnO nanopowders. All of the peaks could be indexed to the hexagonal ZnO wurtzite structure. No diffraction peaks other than ZnO could be found, indicating the high purity of the product. The Brunauer–Emmentt–Teller (BET) method was performed to determine the specific surface areas of the L-ZnO and the S-ZnO, which were determined to be 10.9 and 18.0 m^{-2} g^{-1}, respectively.

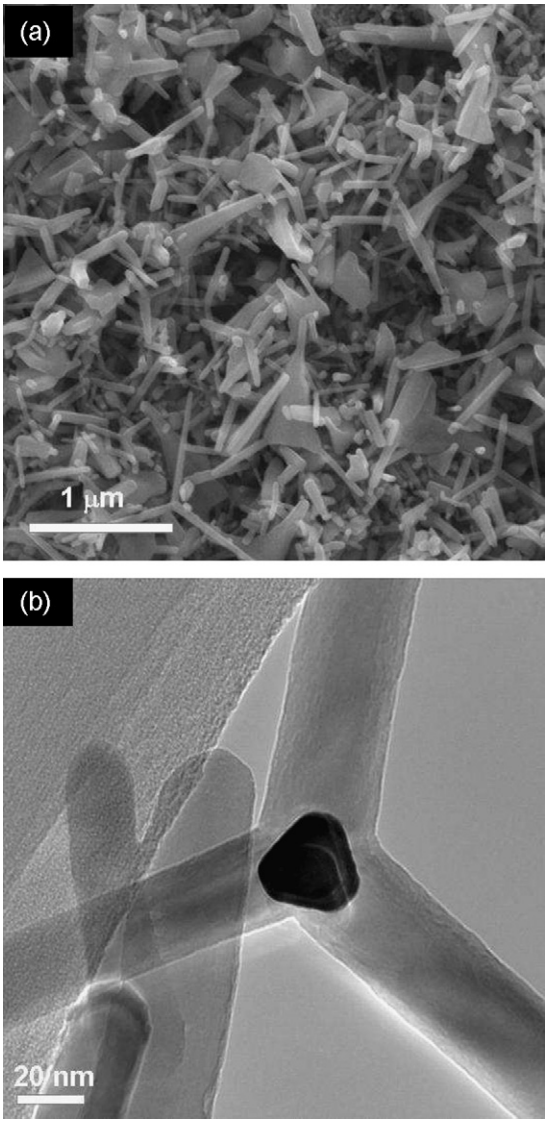

Fig. 1. (a) SEM and (b) TEM images of the tetrapod-like ZnO (L-ZnO) powder fabricated by dc thermal plasma.

This implied that the S-ZnO had a higher dye adsorption ability leading to an increase in light harvesting efficiency.

3.2. The effects of thickness and morphology of tetrapod ZnO photoelectrodes on performance of DSSCs

The photocurrent–voltage (J–V) characteristics of DSSCs constructed from these two tetrapod ZnO (S-ZnO and L-ZnO) photoelectrodes were measured under 100 mW cm^{-2} (AM1.5G). The performance of the DSSC was greatly dependent on the thickness of the ZnO photoelectrode. Fig. 3(a) shows the thickness dependence of the short-current densities (J_{SC}) of the two DSSCs. The current density increased with the thickness for S-ZnO and L-ZnO photoelectrodes. The current density became saturated when thickness of the photoelectrode increased to 25 μm and 42 μm for S-ZnO and L-ZnO, respectively. In comparing of these two tetrapod ZnO DSSC cells, the one composed of S-ZnO possessed a higher current density. This was due to the significantly higher surface area of the S-ZnO photoelectrode. Fig. 3(b) displayed the open-circuit voltage (V_{OC}) of the DSSCs. For both DSSCs, the V_{OC} decreased with an increase in the thickness of photoelectrode. The decrease in the rate of V_{OC} correlated to thickness was less significant for the S-ZnO

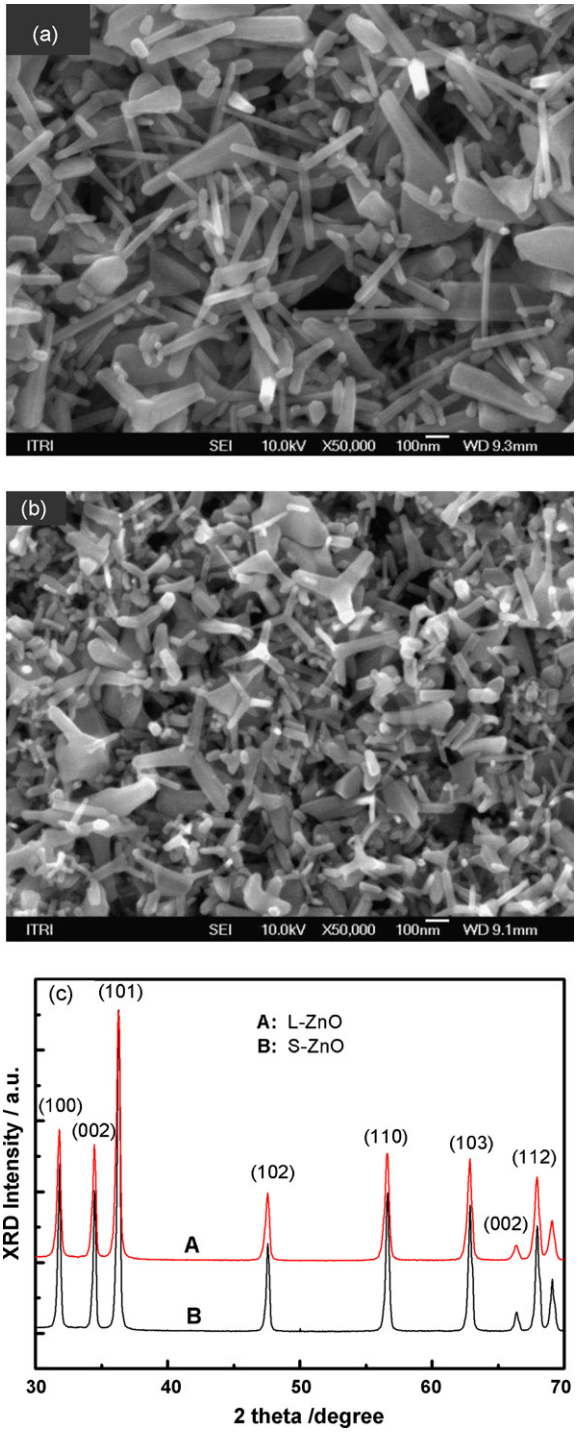

Fig. 2. SEM images of (a) L-ZnO and (b) S-ZnO; and (c) XRD profiles of L-ZnO (A) and the S-ZnO (B).

than it was for the L-ZnO. The decrease in the V_{OC} was generally interpreted as higher charge recombination with a more severely limited mass transport in thicker photoelectrodes. Fig. 3(c) shows that the fill factor (FF) exhibited only a slight decrease with the thickness of photoelectrode. FF is known to be determined by the series resistance of the cell, including the resistances of the FTO, the photoelectrode, the electrolyte, and the counter electrode. In comparison, the FF of DSSCs constructed by 1D material should be relatively higher than DSSCs composed of nanopowders due to improved charge-collection efficiency [28–30]. The series resistance of the tetrapod ZnO photoelectrode could be lower because

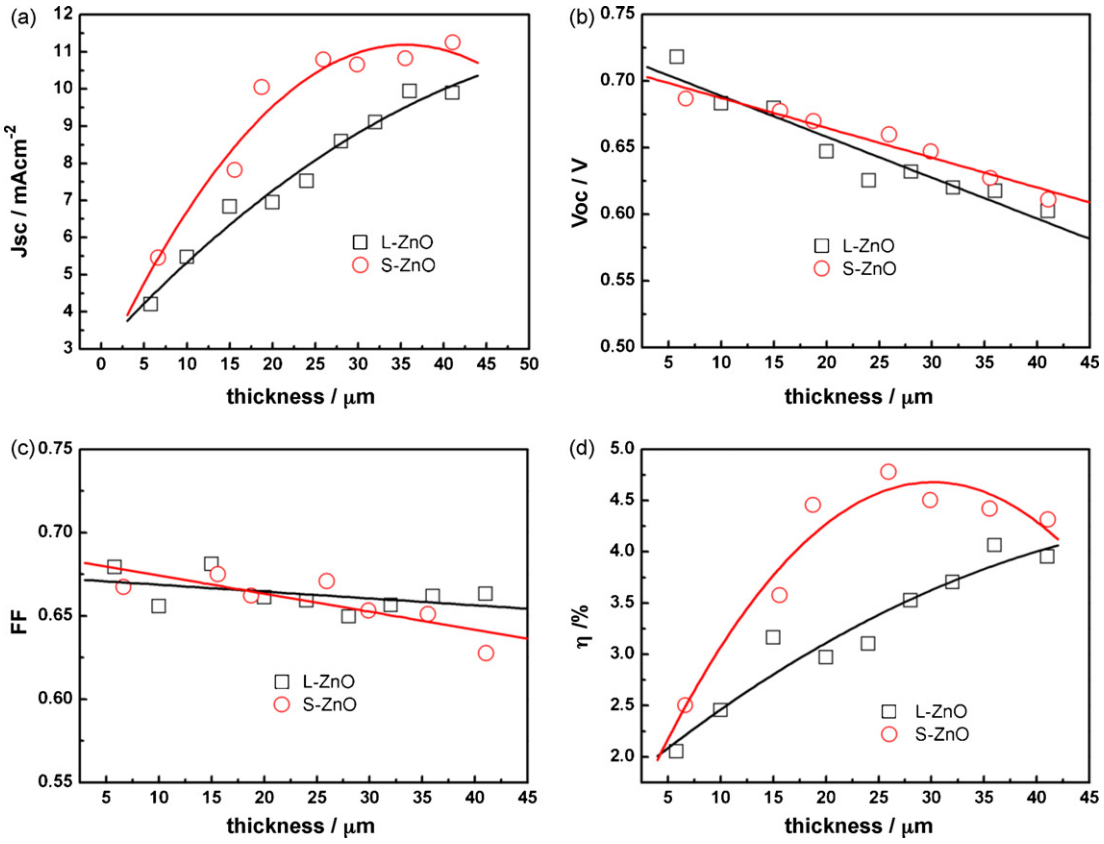

Fig. 3. The effect of ZnO photoelectrode thickness on photovoltaic characteristics of N719-sensitized solar cells based on L-ZnO and S-ZnO photoelectrodes: (a) short-circuit current density (J_{SC}), (b) open-circuit voltage (V_{OC}), (c) fill factor (FF), and (d) overall energy conversion efficiency (η). Electrolyte: 0.1 M LiI, 0.05 M I_2, 0.6 M PmII, and 0.5 M TBP in AN.

the electrons were able to transport through its extended 1D arm rapidly. In addition, the tetrapod ZnO photoelectrode had large pores allowing the ions in the electrolyte to diffuse more easily to the counter electrode. Both factors resulted in higher FF for DSSCs with tetrapod ZnO photoelectrodes. The changes in FF and V_{OC} values corresponding to changes in the thickness of the photoelectrode were less significant for the DSSC constructed by S-ZnO than the one constructed of L-ZnO. This implied that the reduced size and the increased surface area of the S-ZnO did not sacrifice the properties of electron transport. Fig. 3(d) shows the thickness dependence of the overall conversion efficiency. The DSSC composed of S-ZnO had a higher efficiency than the DSSC composed of L-ZnO. This could be attributed to the increase in surface area for dye adsorption, without degradation in the properties of electron transport through the 1D structure of tetrapod ZnO. The thickness of the photoelectrode for N719-sensitized tetrapod ZnO cell was optimized at 26 μm for the S-ZnO DSSC. For the L-ZnO DSSC, the optimized thickness of the photoelectrode was approximately 36 μm. The maximal cell conversion efficiency of the DSSCs was 4.78% and 4.07% for the S-ZnO and L-ZnO DSSC, respectively.

To clarify the morphological effect of ZnO photoelectrodes on the DSSC performance, electrochemical impedance spectroscopy (EIS) was used to characterize the electron transporting properties involved in these complex photovoltaic devices. Impedance measurements were carried out by applying a dc open-circuit voltage (V_{OC}) with a 100 mW cm^{-2} (AM1.5G) illumination. Impedance measurement of the cells was recorded in a frequency range from 10^{-2} Hz to 10^5 Hz with an amplitude of 10 mV. Fig. 4(a) shows the equivalent circuit [31,32] based on a diffusion-recombination model. To extract the electron transport parameters in the ZnO DSSCs, impedance data were fit by the Nyquist plots (Fig. 4(b)). The ZnO DSSCs used for EIS possessed photoelectrodes with a thickness of 25 μm (L). The circuit elements relating to ZnO photoelectrodes included the electron transport resistance ($R_w = r_w L$) in ZnO network, the charge transfer resistance ($R_k = r_k/L$) which related to recombination of electrons at the ZnO/electrolyte interface, and the chemical capacitance ($C_\mu = c_\mu L$) of the ZnO electrode. A number of circuit elements were introduced to modify the equivalent circuit model. They included the series resistance (R_S) of the FTO, the impedance of the diffusion of I_3^- in the electrolyte (Z_N), the charge transfer resistance (R_{Pt}) and the interfacial capacitance (C_{Pt}) at the Pt/electrolyte interface, the charge transfer resistance (R_{FTO}) and the interfacial capacitance (C_{FTO}) at the exposed FTO/electrolyte contact, and the resistance (R_{FZ}) and the capacitance (C_{FZ}) at the FTO/ZnO interface. The electron transport parameters estimated from Nyquist plots are listed in Table 1. They are the electron transport resistance (R_w), charge transfer resistance (R_k), the electron lifetime (τ_{eff}), the effective electron diffusion coefficient (D_{eff}), and the electron diffusion length (L_{eff}) in the investigated tetrapod ZnO photoelectrodes.

As revealed in Table 1, the electron transport resistance (R_w) in S-ZnO was smaller than that of L-ZnO. The charge transfer resistance (R_k) which related to recombination of electrons at the ZnO/electrolyte interface in the S-ZnO device was larger than that of L-ZnO. In combination, the R_k/R_w value of the S-ZnO device was approximately twice that of the L-ZnO device. The higher R_k/R_w value of S-ZnO suggested that a larger number of electrons were injected in S-ZnO. This result may explain the higher observed J_{SC} of S-ZnO than that of L-ZnO. The dye loadings of the L-ZnO and the S-ZnO films was examined by UV–vis spectroscopy (Fig. 4(c)) of the desorbed dye molecules in 10 mM aqueous NaOH solution. The dye loading of the S-ZnO film was higher than that of the L-

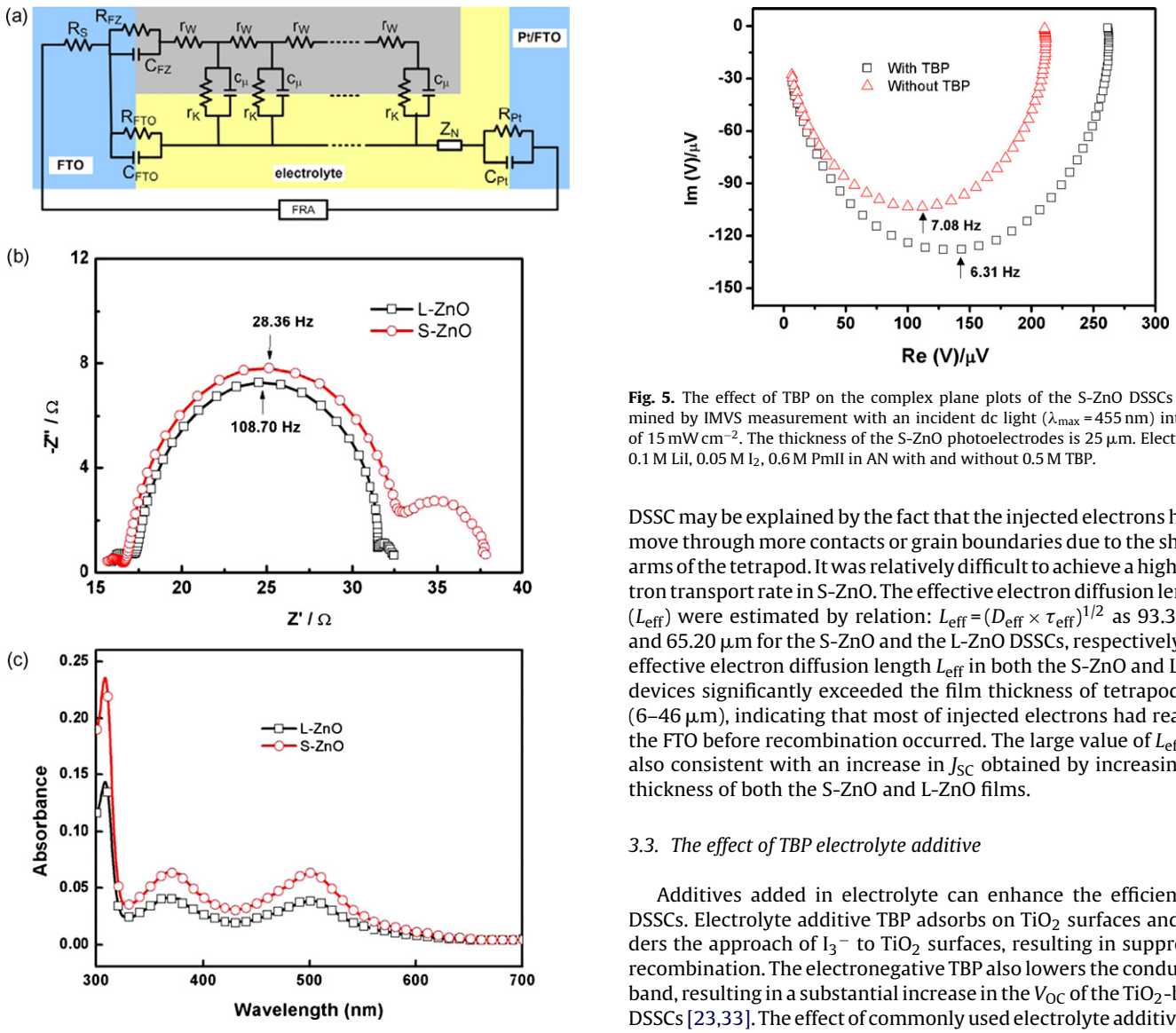

Fig. 4. (a) Equivalent circuit for the simulation of the impedance spectra of the DSSCs. (b) Nyquist plots of L-ZnO and S-ZnO DSSCs determined under an AM 1.5G solar illumination of 100 mW cm^{-2}. The thickness of the ZnO photoelectrode is 25 μm. Electrolyte: 0.1 M LiI, 0.05 M I_2, 0.6 M PmII, and 0.5 M TBP in AN. (c) UV–vis spectroscopy of desorbed dye from the ZnO electrodes.

ZnO. The value of k_{eff} was estimated from the frequency at the top of the central arc ($\omega_{max} = k_{eff}$). The ω_{max} values were 28.36 Hz and 108.70 Hz for the S-ZnO and the L-ZnO devices, respectively. This means that the recombination rate constant (k_{eff}) of the S-ZnO device was lower than that of the L-ZnO one. It is interestingly to note that the electron life time ($\tau_{eff} = 1/k_{eff}$) was extended in the S-ZnO device with respect to the L-ZnO one. This explains the higher observed V_{OC} in the S-ZnO DSSCs. According to the relation: $D_{eff} = (R_k/R_w)L^2 k_{eff}$, the estimated effective electron diffusion coefficient (D_{eff}) of the S-ZnO device was lower than that of the L-ZnO one, due to a the lower k_{eff} of the S-ZnO device. The smaller D_{eff} of S-ZnO

Fig. 5. The effect of TBP on the complex plane plots of the S-ZnO DSSCs determined by IMVS measurement with an incident dc light (λ_{max} = 455 nm) intensity of 15 mW cm^{-2}. The thickness of the S-ZnO photoelectrodes is 25 μm. Electrolyte: 0.1 M LiI, 0.05 M I_2, 0.6 M PmII in AN with and without 0.5 M TBP.

DSSC may be explained by the fact that the injected electrons had to move through more contacts or grain boundaries due to the shorter arms of the tetrapod. It was relatively difficult to achieve a high electron transport rate in S-ZnO. The effective electron diffusion lengths (L_{eff}) were estimated by relation: $L_{eff} = (D_{eff} \times \tau_{eff})^{1/2}$ as 93.32 μm and 65.20 μm for the S-ZnO and the L-ZnO DSSCs, respectively. The effective electron diffusion length L_{eff} in both the S-ZnO and L-ZnO devices significantly exceeded the film thickness of tetrapod ZnO (6–46 μm), indicating that most of injected electrons had reached the FTO before recombination occurred. The large value of L_{eff} was also consistent with an increase in J_{SC} obtained by increasing the thickness of both the S-ZnO and L-ZnO films.

3.3. The effect of TBP electrolyte additive

Additives added in electrolyte can enhance the efficiency of DSSCs. Electrolyte additive TBP adsorbs on TiO_2 surfaces and hinders the approach of I_3^- to TiO_2 surfaces, resulting in suppressed recombination. The electronegative TBP also lowers the conduction band, resulting in a substantial increase in the V_{OC} of the TiO_2-based DSSCs [23,33]. The effect of commonly used electrolyte additives for TiO_2-based DSSCs, i.e. *tert*-butylpyridine (TBP), on the performance of the S-ZnO DSSCs is presented in this section. In order to study the effect of the TBP additive in electrolyte on the electron transport property, intensity-modulated photovoltage spectroscopy (IMVS) was applied to measure the electron life time under open-circuit conditions with a 15 mW cm^{-2} illumination. The IMVS measured the modulation of photovoltage in response to the modulation frequencies of the incident light, which could be expressed as polar coordinates in the complex plane plots.

Fig. 5 shows the IMVS plots of the S-ZnO DSSCs with and without the TBP additive. The mean electron life time could be obtained from the IMVS plot by the equation $\tau_n = 1/2\pi f_{min}$, where f_{min} is the frequency at the lowest imaginary component in the IMVS plots [34,35]. The electron life time and the corresponding cell performance data are listed in Table 2. The value of τ_n of the device without TBP additive was less than that with TBP additive, which meant that electrons were lost rapidly in the DSSC without TBP.

Table 1
Performances and electron transport properties of the L-ZnO and S-ZnO DSSCs determined by photocurrent density–voltage characteristics and electrochemical impedance spectroscopy (EIS) analysis. The thicknesses of photoelectrodes are 25 μm.

ZnO DSSC	η (%)	J_{SC} (mA cm^{-2})	V_{OC} (V)	FF	R_w (Ω)	R_k (Ω)	τ_{eff} (ms)	D_{eff} ($\times 10^{-3}$ cm^2 s^{-1})	L_{eff} (μm)
L-ZnO	3.52	8.59	0.63	0.65	2.21	15.04	9.20	4.62	65.20
S-ZnO	4.78	10.79	0.66	0.67	1.36	18.95	35.26	2.47	93.32

Table 2
The effect of TBP on photovoltaic performances and electron life time of DSSCs.

Electrolyte	η (%)	J_{SC} (mA cm^{-2})	V_{OC} (V)	FF	f_{min} (Hz)	τ_n (ms)
0 M TBP	3.46	9.38	0.59	0.63	7.08	22.5
0.5 M TBP	4.10	8.94	0.67	0.68	6.31	25.2

This could be attributed to the adsorption of TBP on S-ZnO surfaces and the suppression of recombination, which was expected from the higher V_{OC} value of the S-ZnO DSSC containing TBP. Although the J_{SC} of the DSSC with TBP was sacrificed slightly, the V_{OC} and FF were improved. Consequently, the overall conversion efficiency was enhanced by the addition of TBP.

3.4. The effect of lithium cations in electrolytes

In previous research, cations were found to adsorb on the surface of TiO_2 or intercalate the TiO_2 lattice, which change the energetic of the TiO_2 [22]. It is worthy to investigate the effect of additives, in particular lithium cations on performance of ZnO-based DSSCs. The concentration of the TBP additive was fixed at 0.5 M, while the concentration of Li^+ (LiI) was varied over the range of 0–0.1 M. Fig. 6(a) shows the effect of LiI concentration in electrolyte solutions on J_{SC}, FF, V_{OC}, and η of S-ZnO DSSCs. It is apparent that the concentration of Li^+ had a significant influence on J_{SC}. The J_{SC} initially increased from 9.01 to 11.01 mA cm^{-2} with an increase in the concentration of LiI from 0 to 0.05 M. The J_{SC} was saturated with additional LiI. The effect of Li ions is considered similar to that of TiO_2-based DSSCs reported by Watson and Meyer [22]. That is, Li^+ lowered the conduction band of ZnO and promoted electron injection from the excited state of dye molecules, which consequently resulted in an increase in J_{SC}.

The effect of Li^+ on the electron transport characteristics of the DSSCs was investigated by using EIS under open-circuit condition with a 100 mW cm^{-2} illumination. The electron transport properties evaluated from EIS data and the correlated cell performances are summarized in Table 3. The Li^+ cations did not have a significant influence on R_w and R_k values. On the other hand, Fig. 6(b) shows that the characteristic frequency peaks in the Bode plots had shifted with the concentration of LiI. A typical Bode plot exhibits three characteristic frequency peaks which could be attributed to the Nernst diffusion in the electrolyte, the electron transfer at the ZnO/electrolyte interface, and the redox charge transfer at the counter electrode [36]. The frequency peak representing the electron transfer at the ZnO/electrolyte interface (1–10^3 Hz) initially shifted to a lower frequency with an increase in the concentration of LiI, where it remained constant when the concentration of LiI was greater than 0.05 M. The inverse of the characteristic frequency ($1/\omega_{max}$) is equal to the electron life time (τ_{eff}) of the ZnO photoelectrode [37]. The correlation between J_{SC} and τ_{eff} is shown in Fig. 6(c), indicating that the electron lifetime initially increased with an increase in the concentration of LiI where it remained almost unchanged, with a further increase in the concentration of LiI (greater than 0.05 M). Without significant change of R_w or R_k, τ_{eff} becomes the dominating factor affecting J_{SC}. These factors may explain the relatively good correlation between J_{SC} and τ_{eff}.

Li^+ ions do not have significant effect on V_{OC} and FF. As for the conversion efficiency, η, LiI concentration has a similar effect to that of J_{SC}. Therefore, the effect of Li ions on η can be attributed mainly to J_{SC}.

3.5. Concentration effect of I_2 in electrolyte

It was reported that the concentration of I^- had no influence on the performance of DSSC. The performance of the DSSC was dominated by the concentration of I_3^-, not I^- [24,25]. The redox couple in the electrolyte, normally I^-/I_3^-, transfers charge between the photoelectrode and the counter electrode, resulting in redox reaction at the electrodes. The concentrations of I^- and I_3^- were expected to affect the performance of DSSC. Fig. 7 depicts the influence of the concentration of I_2 on various parameters of DSSCs obtained through optimized S-ZnO thickness of photoelectrode 25 μm. The

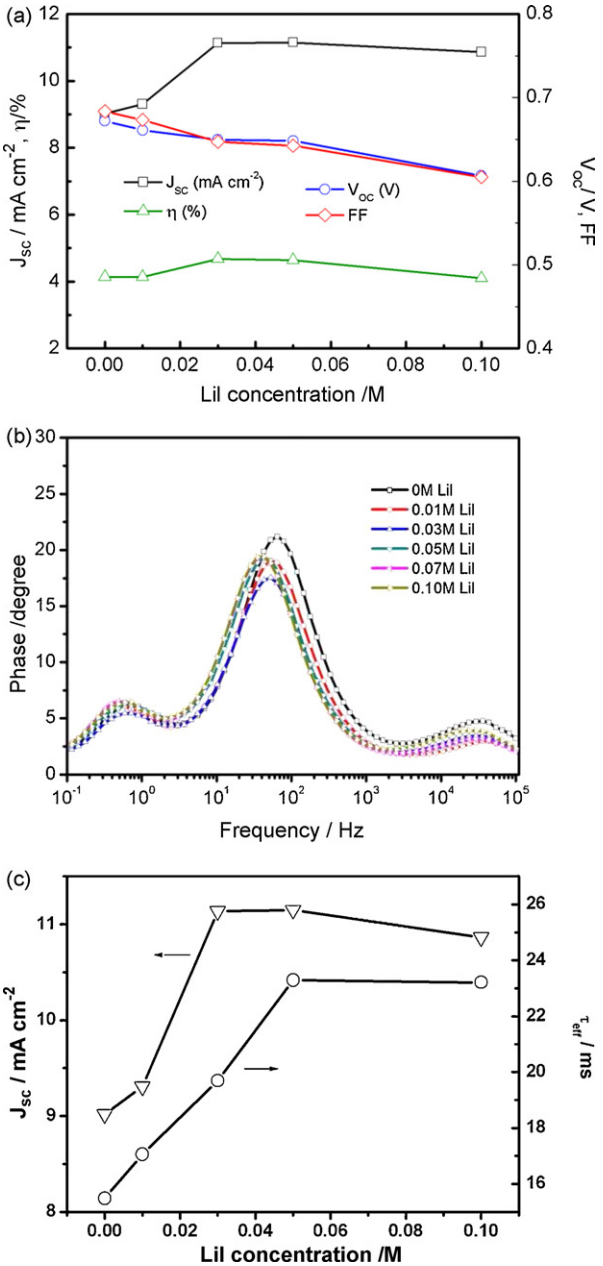

Fig. 6. (a) Dependence of short-circuit current density (J_{SC}), open-circuit voltage (V_{OC}), fill factor (FF) and overall energy conversion efficiency for S-ZnO-based DSSCs on the concentration LiI of the electrolyte. (b) Bode plots of the impedance data of the S-ZnO DSSCs with different concentrations of LiI. (c) Electron lifetime (τ_{eff}) and short-circuit current density (J_{SC}) vs DSSC containing different concentrations of LiI. Electrolyte: LiI (0 M, 0.01 M, 0.03 M, 0.05 M, 0.10 M), 0.05 M I_2, 0.6 M PmII, and 0.5 M TBP in AN.

Table 3
Photovoltaic performances, electron recombination rate constant (k_{eff}), and electron life time (τ_{eff}) evaluated by EIS.

Electrolyte	η (%)	J_{SC} (mA cm^{-2})	V_{OC} (V)	FF	R_w (Ω)	R_k (Ω)	k_{eff} (Hz)	τ_{eff} (ms)
0 M LiI	4.14	9.02	0.67	0.68	1.26	19.01	64.58	15.48
0.05 M LiI	4.68	11.14	0.65	0.65	1.36	18.95	52.64	19.00

J_{SC} of the DSSCs depended strongly on the concentration of I_2. The J_{SC} increased with an increase in the concentration of I_2, exhibiting a peak value at a concentration of 0.07 M I_2, at which point, it decreased dramatically with additional I_2. A sufficient concentration of I^-/I_3^- redox couple is needed for the cell operation. Interaction between I^- and I_3^- is described by reaction (1).

$$I^- + I_2 \leftrightarrow I_3^- \quad (1)$$

An increase in I_2 concentration led to an increase in I_3^- concentration. Therefore, J_{SC} initially increases with I_2 concentration. However, an excess of I_3^- tended to react with electrons at the surfaces of ZnO photoelectrodes, according to reaction (2).

$$I_3^- + 2e^- \leftrightarrow 3I^- \quad (2)$$

V_{OC} and FF values declined slightly with an increase in the concentration of I_2. The parameters estimated from the impedance spectra are listed in Table 4. The electron transport resistance (R_w) (approximately 1 Ω) fluctuated with an increase in concentration of I_2. This indicated that the concentration of I_2 had not significantly affected the electron transport characteristics at the S-ZnO photoelectrode. On the other hand, the recombination resistances R_k decreased with an increase in concentration of I_2. The decrease in R_k indicated that the interfacial recombination of electrons had increased, which was consistent with a decrease in the FF of the DSSCs with increasing I_2 concentration. This result suggests that the enhanced interfacial recombination of electrons had decreased electron density in ZnO, which could explain the decrease in V_{OC} with an increase in the concentration of I_2. According to reaction (1), the concentration of I_3^- at ZnO/electrolyte interfaces increased with the concentration of I_2 added to the electrolyte [38]. As a consequence, the recombination rate constant with I_3^- (k_{eff}) in the S-ZnO DSSC was raised. Therefore, the electron life time (τ_{eff}) decreased with an increase in the concentration of I_3^-, as shown in Table 4. The observed decline in V_{OC} could also be attributed

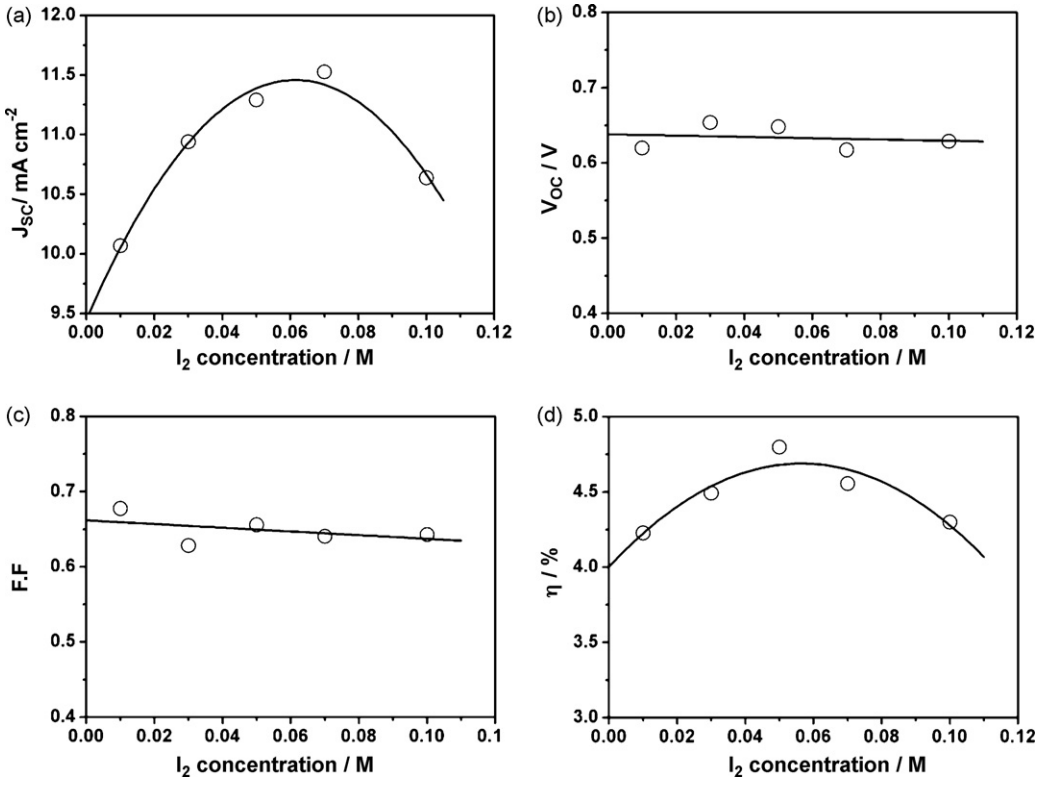

Fig. 7. Photovoltaic characteristics of S-ZnO DSSCs as a function of I_2 concentration: (a) short-circuit current density (J_{SC}), (b) open-circuit voltage (V_{OC}), (c) fill factor (FF), and (d) overall energy conversion efficiency (η). The thickness of the S-ZnO photoelectrode is 25 μm. Electrolyte: 0.1 M LiI, I_2 (0.01 M, 0.03 M, 0.05 M, 0.07 M, 0.10 M), 0.6 M PmII, and 0.5 M TBP in AN.

Table 4
The effect of I_2 concentration on electron transport properties of ZnO DSSCs. The thickness of the S-ZnO photoelectrodes is 25 μm.

I_2 (M)	R_w (Ω)	R_k (Ω)	k_{eff} (s^{-1})	τ_{eff} (ms)	D_{eff} (×10^{-3} cm^2 s^{-1})	L_{eff} (μm)
0.01	0.40	23.99	24.77	40.36	9.23	192.98
0.03	1.23	20.88	31.18	32.07	3.31	103.02
0.05	0.94	9.73	39.78	25.14	2.57	80.45
0.07	1.89	7.08	74.39	13.44	1.74	48.32

to a decrease in τ_{eff} values of DSSCs containing large amount of I_3^-.

The effective diffusion coefficient (D_{eff}) was calculated with a fixed thickness of S-ZnO photoelectrode 25 μm (L). The obtained D_{eff} value decreased with the concentration of I_2. Calculations based on the aforementioned equation: $L_{eff} = (D_{eff} \times \tau_{eff})^{1/2}$, the L_{eff} of S-ZnO DSSCs were found to decrease with the I_2 concentration due to a decrease in D_{eff} and τ_{eff}. The electron diffusion length (L_{eff}) illustrated the competition between the recombination and the collection of electrons. The L_{eff} values had a declining trend with increases in I_2 concentrations. Although all the estimated L_{eff} values (48.32–192.98 μm) were longer than the thickness of the ZnO photoelectrode (25 μm), J_{SC} exhibited a peak value at a concentration of 0.07 M I_2. This suggests that the collection of electrons was efficient when L_{eff} was approximately two times greater than the film thickness of photoelectrode. The decrease in the J_{SC} with the further addition of I_2 was caused by the increase in recombination.

4. Conclusions

We prepared two tetrapod-like ZnO nanopowders with different morphologies using dc thermal plasma synthesis. The short-circuit current density and the efficiency of the S-ZnO DSSC had improved in comparison with L-ZnO DSSC, due to its increased surface area and enhanced electron transport characteristics. The electron life time of the S-ZnO photoelectrode was significantly prolonged compared with the photoelectrode composed of L-ZnO. As for electrolyte additives, IMVS measurement revealed that TBP had prolonged the electron life time in ZnO DSSCs. The J–V characteristics depend greatly on the concentration of LiI and I_2. EIS measurements illustrated that lithium cations (less than 0.05 M) in electrolytes lengthen the electron life time of the S-ZnO DSSCs and consequently enhanced the corresponding short circuit current values. Furthermore, the electron life time and effective electron diffusion length decreased with an increase in the concentration of I_3^-. This led to slightly reduced V_{OC} and FF, whereas the corresponding J_{SC} values increased significantly. Finally, we identify the efficiency of the S-ZnO DSSC was improved because its effective diffusion length was greater than the thickness of S-ZnO photoelectrodes.

Acknowledgements

We gratefully acknowledge the financial support of Bureau of Energy, Ministry of Economics Affairs, Taiwan, and the National Science Council of Taiwan.

References

[1] M. Gratzel, J. Photochem. Photobiol. A: Chem. 168 (2004) 235.
[2] M.K. Nazeeruddin, F. De Angelis, S. Fantacci, A. Selloni, G. Viscardi, P. Liska, S. Ito, B. Takeru, M.G. Gratzel, J. Am. Chem. Soc. 127 (2005) 16835.
[3] J. van de Lagemaat, A.J. Frank, J. Phys. Chem. B 105 (2001) 11194.
[4] Q. Wang, S. Ito, M. Gratzel, F. Fabregat-Santiago, I. Mora-Sero, J. Bisquert, T. Bessho, H. Imai, J. Phys. Chem. B 110 (2006) 25210.
[5] Y. Saito, S. Kambe, T. Kitamura, Y. Wada, S. Yanagida, Solar Energy Mater. Solar Cells 83 (2004) 1.
[6] K. Hara, T. Horiguchi, T. Kinoshita, K. Sayama, H. Sugihara, H. Arakawa, Solar Energy Mater. Solar Cells 64 (2000) 115.
[7] K. Sayama, H. Sugihara, H. Arakawa, Chem. Mater. 10 (1998) 3825.
[8] R. Katoh, A. Furube, T. Yoshihara, K. Hara, G. Fujihashi, S. Takano, S. Murata, H. Arakawa, M. Tachiya, J. Phys. Chem. B 108 (2004) 4818.
[9] M. Quintana, T. Edvinsson, A. Hagfeldt, G. Boschloo, J. Phys. Chem. C 111 (2007) 1035.
[10] Q.F. Zhang, C.S. Dandeneau, X.Y. Zhou, G.Z. Cao, Adv. Mater. 21 (2009) 4087.
[11] Y.F. Gao, M. Nagai, T.C. Chang, J.J. Shyue, Cryst. Growth Des. 7 (2007) 2467.
[12] A.B.F. Martinson, J.W. Elam, J.T. Hupp, M.J. Pellin, Nano Lett. 7 (2007) 2183.
[13] M. Law, L.E. Greene, J.C. Johnson, R. Saykally, P.D. Yang, Nat. Mater. 4 (2005) 455.
[14] C.H. Ku, J.J. Wu, Nanotechnology 18 (2007) 505706.
[15] C.Y. Jiang, X.W. Sun, G.Q. Lo, D.L. Kwong, J.X. Wang, Appl. Phys. Lett. 90 (2007) 263501.
[16] E. Hosono, S. Fujihara, I. Honna, H.S. Zhou, Adv. Mater. 17 (2005) 2091.
[17] T.P. Chou, Q.F. Zhang, G.E. Fryxell, G.Z. Cao, Adv. Mater. 19 (2007) 2588.
[18] Q.F. Zhang, T.P. Chou, B. Russo, S.A. Jenekhe, G. Cao, Adv. Funct. Mater. 18 (2008) 1654.
[19] Q.F. Zhang, T.R. Chou, B. Russo, S.A. Jenekhe, G.Z. Cao, Angew. Chem. Int. Ed. 47 (2008) 2402.
[20] K. Keis, E. Magnusson, H. Lindstrom, S.E. Lindquist, A. Hagfeldt, Solar Energy Mater. Solar Cells 73 (2002) 51.
[21] W.-H. Chiu, C.-H. Lee, H.-M. Cheng, H.-F. Lin, S.-C. Liao, J.-M. Wu, W.-F. Hsieh, Energy Environ. Sci. 2 (2009) 694.
[22] D.F. Watson, G.J. Meyer, Coord. Chem. Rev. 248 (2004) 1391.
[23] T. Hoshikawa, T. Ikebe, R. Kikuchi, K. Eguchi, Electrochim. Acta 51 (2006) 5286.
[24] V. Suryanarayanan, K.M. Lee, J.G. Chen, K.C. Ho, J. Electroanal. Chem. 633 (2009) 146.
[25] S. Nakade, T. Kanzaki, W. Kubo, T. Kitamura, Y. Wada, S. Yanagida, J. Phys. Chem. B 109 (2005) 3480.
[26] H.X. Wang, J. Bell, J. Desilvestro, M. Bertoz, G. Evans, J. Phys. Chem. C 111 (2007) 15125.
[27] H.F. Lin, S.C. Liao, S.W. Hung, J. Photochem. Photobiol. A: Chem. 174 (2005) 82.
[28] B. Tan, Y.Y. Wu, J. Phys. Chem. B 110 (2006) 15932.
[29] E. Enache-Pommer, J.E. Boercker, E.S. Aydil, Appl. Phys. Lett. 91 (2007) 123116.
[30] K. Zhu, N.R. Neale, A. Miedaner, A.J. Frank, Nano Lett. 7 (2007) 69.
[31] J. Bisquert, J. Phys. Chem. B 106 (2002) 325.
[32] M. Adachi, M. Sakamoto, J.T. Jiu, Y. Ogata, S. Isoda, J. Phys. Chem. B 110 (2006) 13872.
[33] S.E. Koops, B.C. O'Regan, P.R.F. Barnes, J.R. Durrant, J. Am. Chem. Soc. 131 (2009) 4808.
[34] T. Oekermann, D. Zhang, T. Yoshida, H. Minoura, J. Phys. Chem. B 108 (2004) 2227.
[35] J. Kruger, R. Plass, M. Gratzel, P.J. Cameron, L.M. Peter, J. Phys. Chem. B 107 (2003) 7536.
[36] D.B. Kuang, S. Ito, B. Wenger, C. Klein, J.E. Moser, R. Humphry-Baker, S.M. Zakeeruddin, M. Gratzel, J. Am. Chem. Soc. 128 (2006) 4146.
[37] J.J. Wu, G.R. Chen, H.H. Yang, C.H. Ku, J.Y. Lai, Appl. Phys. Lett. 90 (2007) 213109.
[38] K. Hara, T. Horiguchi, T. Kinoshita, K. Sayama, H. Arakawa, Solar Energy Mater. Solar Cells 70 (2001) 151.